Interlayer coupling in $Fe/Fe_{1-x}Si_x$ superlattices

Yasushi Endo,* Osamu Kitakami, and Yutaka Shimada
Section of Solid State Electron Physics, Research Institute for Scientific Measurements, Tohoku University, 2-1-1 Katahira, Aoba, Sendai 980-8577, Japan

(Received 3 February 1998; revised manuscript received 15 July 1998)

Interlayer coupling has been investigated for a series of $Fe/Fe_{1-x}Si_x$ ($0.4 \leqslant x \leqslant 1.0$) superlattices. The layer of $Fe_{1-x}Si_x$ in the lattices is ferromagnetic for $x < 0.5$ and causes ferromagnetic coupling between Fe layers for all spacer thicknesses investigated here. As the Si content increases above $x = 0.5$, the layer becomes nonmagnetic and simultaneously our current in the plane of the sample and current perpendicular to the sample plane measurements suggest that the spacer rapidly changes its conduction property from metallic to highly resistive. Variations of the interlayer magnetic coupling as a function of spacer layer thickness for the spacer compositions above $x = 0.5$ are similar to each other; namely, with an increase of the spacer thickness the interlayer coupling is initially ferromagnetic, then antiferromagnetic, and finally becomes noncoupling. Moreover, the temperature dependence of the bilinear and biquadratic coupling constants, $J_1(T)$ and $J_2(T)$ which were obtained by numerical fitting, varies sensitively with x. Assuming that the conduction of the spacers ranges from metallic to insulating as x increases, all these coupling behaviors can be described qualitatively by the quantum interference model formalized by Bruno. Furthermore, we found that the coupling strength is enhanced dramatically with increase of x of $Fe_{1-x}Si_x$. [S0163-1829(99)11405-X]

I. INTRODUCTION

Since the discovery of indirect exchange coupling between ferromagnetic layers separated by a nonmagnetic metal spacer,[1,2] numerous studies have been performed for magnetic metal/nonmagnetic metal superlattices. Recently, renewed interest in this field has been brought about by observation of interlayer coupling across a nonmetallic spacer. Toscano *et al.* found interlayer coupling in Fe/Si/Fe trilayers, and they speculate that the coupling is mediated by the phonon-assisted hopping electrons in the localized states of amorphous Si (a-Si).[3–5] In general, however, severe interdiffusion occurs at Fe/Si interfaces during sample preparation, resulting in the formation of various kinds of silicides. Upon precise structural characterizations it was claimed that a metallic silicide layer with the CsCl structure produced by interdiffusion at the interface mediates the coupling through the Ruderman-Kittel-Kasuya-Yoshida (RKKY) interaction.[6–11] Another proposed model is that thermally excited carriers in the narrow gap semiconducting spacer contribute to the coupling.[12] Thus the origin of the interlayer coupling in Fe/Si superlattices has been very controversial and is still an open question. The most crucial point which makes this problem difficult is the complex diffused structure in the Si spacer. According to our precise structural analyses,[10] however, interdiffusion at the interface can be considerably suppressed by using an Fe-Si alloy as spacer material. Hence it is expected that investigation of various kinds of $Fe/Fe_{1-x}Si_x$ superlattices will give very useful information on the coupling mechanism of Fe/Si superlattices.

In this paper, we explore the magnetic and electric properties of various kinds of $Fe/Fe_{1-x}Si_x$ superlattices ($0.4 \leqslant x \leqslant 1.0$), and the mechanism of interlayer coupling is discussed on the basis of the typical theoretical coupling models reported so far.

II. EXPERIMENTAL

A series of $Fe/Fe_{1-x}Si_x$ ($0.4 \leqslant x \leqslant 1.0$) superlattices was grown on surface oxidized Si(100) substrates at ambient temperature in a dc magnetron sputtering system, with a base pressure less than 6×10^{-7} Torr and an argon gas pressure of 3 mTorr. The composition x of Fe-Si alloys was controlled by placing Fe chips on a $Fe_{0.27}Si_{0.73}$ or a Si target, and the film compositions were determined by the x-ray photoelectron spectroscopy. The deposition rates for Fe and $Fe_{1-x}Si_x$ layers were 1.9–2.1 and 0.4–0.6 Å/s, respectively. Prior to preparation of various kinds of $Fe/Fe_{1-x}Si_x$ superlattices, we explored physical properties of 1000 Å thick $Fe_{1-x}Si_x$ single layers. From Table I, $Fe_{1-x}Si_x$ becomes paramagnetic for $x > 0.5$ and the resistivity increases rapidly with x. The superlattices were grown with the Fe layer thickness t_F fixed at 30 Å and the nominal $Fe_{1-x}Si_x$ layer thickness t_s varied from 5–70 Å, with 22 bilayers. The periodic and crystallographic structures of the $Fe/Fe_{1-x}Si_x$ superlattices were characterized by both low- and high-angle x-ray diffraction (XRD) using Cu $K\alpha$ radiation. The superlattice period (Λ) was evaluated by the kinematical Bragg's law $\Lambda = l\lambda/2 \sin\theta$ for the lth order reflection, here λ is the x-ray wavelength and θ is the observed diffraction angle. Since the lower order reflections

TABLE I. Physical properties of $Fe_{1-x}Si_x$ layers after annealing at 200 °C for 2 h. $\rho_{\text{multi.}}$ is the resistivity determined by fitting procedures for the dependence of ρ as a function of the spacer thickness.

$Fe_{1-x}Si_x$ spacer	M_s (G)	ρ_{sl} ($\mu\Omega$ cm)	$\rho_{\text{multi.}}$ ($\mu\Omega$ cm)
$Fe_{0.27}Si_{0.73}$	0	6370	>10 000
$Fe_{0.37}Si_{0.63}$	0	510	500
$Fe_{0.46}Si_{0.54}$	0	300	200
$Fe_{0.54}Si_{0.46}$	530	200	100

are seriously influenced by the refraction effect, we first calculated Λ for all detected Bragg reflections and then accurately determined the saturation (true) period for larger l.[13] The validity of this method was also confirmed by direct observations of $Fe/Fe_{1-x}Si_x$ cross sections using a transmission electron microscope. The crystalline coherence length (ξ) was estimated from the full width at half maximum (FWHM) of a Fe(110) diffraction peak by using the following Scherrer's relation;[14] $\xi = 0.9\lambda / B\cos\theta_B$ and $B = \sqrt{B_M^2 - B_S^2}$, where θ_B denotes the Bragg angle of Fe(110), and B_M and B_S are the FWHM values for $Fe/Fe_{1-x}Si_x$ superlattices and the standard bulk Fe, respectively. The estimated ξ well represents the crystalline coherence length of the superlattices. In fact, the value coincides with the thickness of the deposited Fe layers when $Fe_{1-x}Si_x$ spacer is purely amorphous or severely disordered, as already pointed out by Fullerton *et al.*[6]

The magnetic properties of most samples were measured by a vibrating-sample magnetometer with a maximum field of 15 kOe. For some samples with extremely strong antiferromagnetic coupling, a superconducting quantum interference device magnetometer with a field of 50 kOe was utilized in order to fully saturate the samples. Ferromagnetic resonance (FMR) measurements were also carried out with an electronic paramagnetic resonance spectrometer operating at the frequency of 9.1 GHz in order to confirm and evaluate the ferromagnetic and antiferromagnetic interlayer coupling in the superlattices.[15,16] From the magnetization measurements, the bilinear coupling constant J_1 can be roughly evaluated by $J_1 = M_s H_s t_F/4$ if the biquadratic coupling constant J_2 is negligible, where M_s is the saturation magnetization and H_s is the saturation field. The constant J_1 can be also estimated from FMR measurements as $J_1 = (H' - H^*) M_s t_F$, where H' and H^* are the resonance fields for optical and acoustic modes, respectively. J_1 values evaluated by the above two methods roughly coincided with each other for most of our samples. For more quantitative discussions, however, the biquadratic coupling constant J_2 has to be taken into account in the total-energy expression for $Fe/Fe_{1-x}Si_x$ superlattices, as will be described later.

The electric resistance of the samples was measured by current perpendicular to plane (CPP) geometry using crossed electrode junctions in order to avoid the shunting effect of current in plane (CIP) geometry due to a very large difference in the electric resistivities between Fe layers and $Fe_{1-x}Si_x$ layers. The junction size was designed to realize uniform current flow over the junction area, typically about $5 \times 5\ \mu m^2$. The details for the junction design and measurements are described elsewhere.[11]

III. RESULTS AND DISCUSSION

A. Dependence of interlayer coupling on spacer composition

Prior to preparation of $Fe/Fe_{1-x}Si_x$ superlattices, we first investigated the crystal structures and the physical properties of 1000 Å thick $Fe_{1-x}Si_x$ ($0.46 \leqslant x \leqslant 1.0$) single layers. The XRD scans showed no distinct diffractions for all samples even after annealing at 200 °C for 2 h, indicating that the films are amorphous. Table I lists the saturation magnetization and the electric resistivity (ρ) of the $Fe_{1-x}Si_x$ layers. As

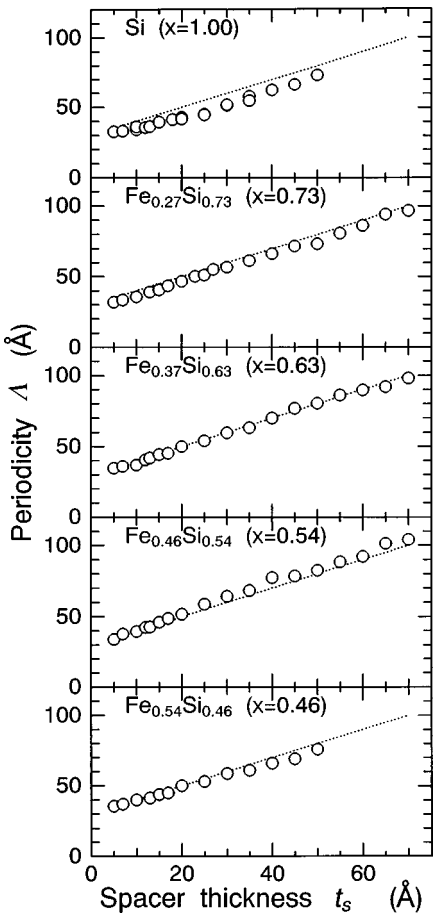

FIG. 1. Dependence of superlattice period (Λ_m) as a function of the spacer thickness (t_s) for $[Fe(30\,Å)/Fe_{1-x}Si_x(t_s\,Å)]_{22}$ ($x = 0.46, 0.54, 0.63, 0.73, 1.00$) superlattices. Dotted lines show the designed values without any interdiffusion. It is noted that the interdiffusion at the interfaces is remarkably reduced for $x \leqslant 0.73$.

expected, the resistivity rapidly increases with the Si content and the films become paramagnetic for $x \geqslant 0.5$ at room temperature.

Figure 1 compares the superlattice period (Λ_m) of the $Fe/Fe_{1-x}Si_x$ with the designed one ($\Lambda_d = t_{Fe} + t_s$) as a function of the spacer thickness. As can be noticed in this figure, Λ_m is somewhat smaller than Λ_d for pure Si ($x = 1$), suggesting that interdiffusion occurs at the interfaces. In contrast, Λ_m well coincides with Λ_d for $x \leqslant 0.73$, indicating that the interdiffusion at the interfaces is considerably suppressed. In fact, their saturation magnetization is in good agreement with the bulk value of α-Fe (1717 G) and is independent of the spacer thickness. The crystalline coherence length ξ of the superlattices is greatly affected by the Si content of the spacer as shown in Fig. 2. It is expected that if the spacer is amorphous, ξ is equal to the individual Fe layer thickness t_{Fe} (30 Å). This is actually observed in $Fe/Fe_{1-x}Si_x$ ($x \geqslant 0.73$) superlattices for $t_s > 20$ Å, implying that the spacer layer is either amorphous or sufficiently disordered to limit crystalline coherence within the Fe layer thickness. For $t_s \leqslant 20$ Å, however, ξ increases to ~160 Å. This indicates that the spacer layer is crystalline. On the other hand, the spacer layer is crystalline over the whole spacer thickness for $x \leqslant 0.63$ because the coherence length far exceeds the indi-

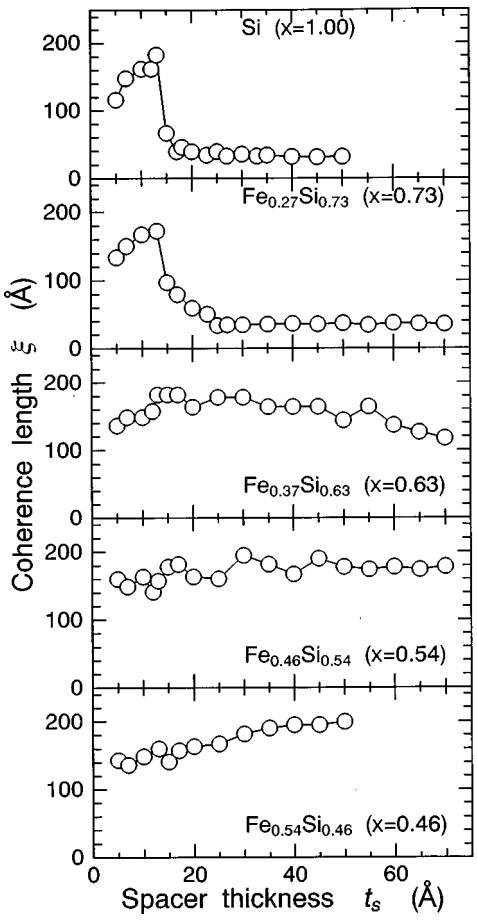

FIG. 2. Dependence of the coherence length (ξ) as a function of the spacer thickness (t_s) for $[Fe(30\,Å)/Fe_{1-x}Si_x(t_s\,Å)]_{22}$ ($x=0.46$, 0.54, 0.63, 0.73, 1.00) superlattices.

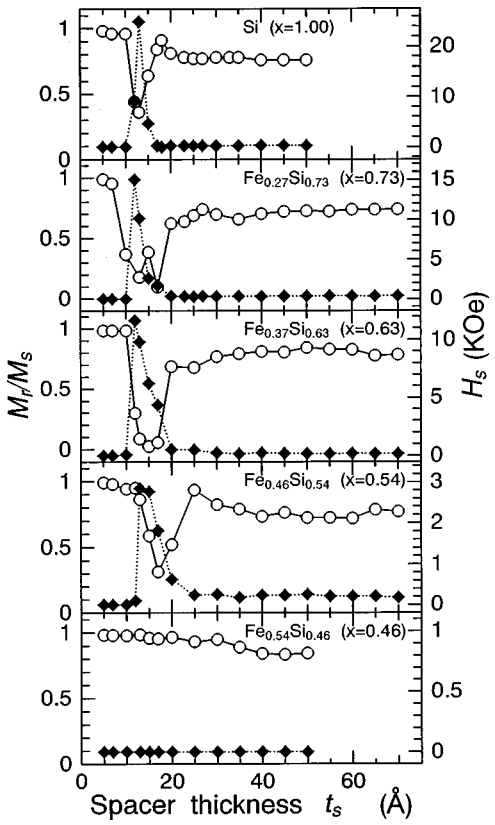

FIG. 3. Dependence of the remanence ratio (M_r/M_s) and the saturation field (H_s) as a function of the spacer thickness (t_s) for $[Fe(30\,Å)/Fe_{1-x}Si_x(t_s\,Å)]_{22}$ ($x=0.46$, 0.54, 0.63, 0.73, 1.00) superlattices. Empty circles (○) and solid diamonds (◆) indicate M_r/M_s and H_s, respectively.

vidual Fe layer thickness. This suggests that the spacer structure is stabilized by epitaxial constraints to the α-Fe layer.

As shown in Fig. 3, the interlayer coupling exhibits very similar dependence on spacer thickness for all $Fe/Fe_{1-x}Si_x$ ($x \geqslant 0.54$) superlattices irrespective of x; that is, ferromagnetic coupling for $t_s < 10$ Å, antiferromagnetic (AF) coupling for $10\,Å < t_s < 20\,Å$, and noncoupling for $t_s > 20$ Å. In particular, in the Si spacer, the coupling state for $10\,Å < t_s < 20\,Å$ changes from the antiferromagnetic state to ferromagnetic state.[17] All these coupling behaviors as a function of spacer thickness were also confirmed by FMR measurements. It is noticed that saturation field H_s for AF coupled films greatly depends on the spacer composition; namely, H_s drastically increases with x. Fullerton *et al.* found interlayer coupling for the Fe/Si superlattices with ξ larger than t_{Fe}, and concluded that the coupling is mediated by a metallic iron silicide layer formed by interdiffusion.[6–8] Moreover, they speculated that the disappearance of interlayer coupling for $t_{Si} > 20$ Å where ξ was limited to t_{Fe} could be attributed to the amorphous semiconducting or insulating character of the spacer which would increase the spin-flopping probability.[6] We note that the above discussion seems to be valid only for $x \geqslant 0.73$ but not for $x \leqslant 0.63$, because the silicide spacer with $x \leqslant 0.63$ is crystalline for all thickness regions, as shown in Fig. 2. A few reports claim that the AF coupling found in Fe/Si superlattices is mediated by a metallic B_2-FeSi diffused spacer.[18] This conclusion was mainly derived from the observation of the forbidden Fe(001) spot in an electron-diffraction pattern in addition to analysis of soft x-ray fluorescence spectra. In contrast to this observation, all of our AF coupled $Fe/Fe_{1-x}Si_x$ superlattices showed no x-ray and electron-diffraction spots due to the ordered phase, such as the B_2 or DO_3 phase; namely, all diffraction spots of our samples were ascribed to α-Fe (see Fig. 4). From these results, we can conclude that the B_2 or DO_3 ordered phase is not dominant in our samples. This result suggests that phases other than metallic B_2-FeSi can contribute to AF coupling of $Fe/Fe_{1-x}Si_x$ superlattices. Further discussions on the coupling mechanism will be made in the next section.

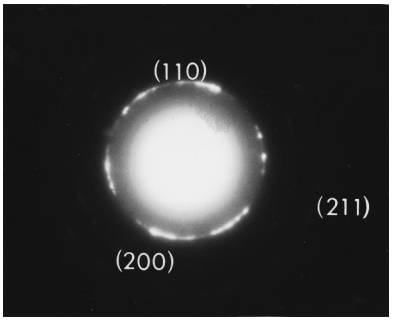

FIG. 4. The diffraction pattern of a $[Fe(30\,Å)/Fe_{0.37}Si_{0.63}(15\,Å)]_{22}$ superlattice. All diffractions are ascribed to α-Fe.

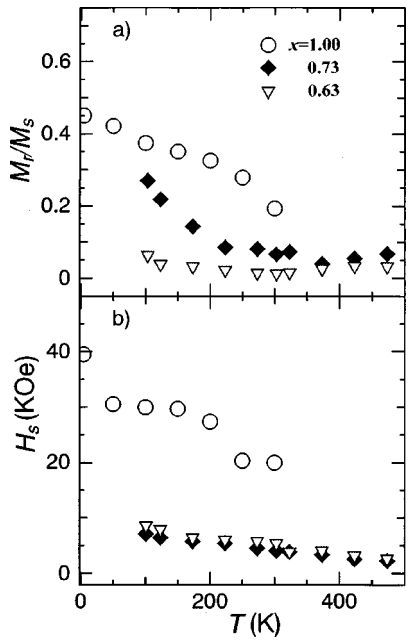

FIG. 5. Temperature dependences of the remanence ratio (M_r/M_s) and the saturation field (H_s) for antiferromagnetically coupled $[\mathrm{Fe}(30\,\text{Å})/\mathrm{Fe}_{1-x}\mathrm{Si}_x(t_{\mathrm{AF}}\,\text{Å})]_{22}$ ($x=0.63$, 0.73, 1.00) superlattices. Empty circles (○), solid diamonds (◆) and empty triangles (▽), respectively, show the data for $x=1.00$, 0.73, and 0.63.

B. Mechanism of interlayer coupling

In the previous report, we presented the resistivity of $\mathrm{Fe}_{1-x}\mathrm{Si}_x$ films obtained by (CIP) measurements of $\mathrm{Fe}/\mathrm{Fe}_{1-x}\mathrm{Si}_x$ superlattices varying the thickness of $\mathrm{Fe}_{1-x}\mathrm{Si}_x$ spacers and numerical fitting.[11] Typical results are given in Table I together with the resistivity of $\mathrm{Fe}_{1-x}\mathrm{Si}_x$ single layers. As shown in Table I, the resistivity of $\mathrm{Fe}_{1-x}\mathrm{Si}_x$ spacers ($\rho_{\mathrm{multi.}}$ in the table) estimated by fitting agrees well with that of the single layers (ρ_{sl} in the table). It should be stressed here that the electric properties of the spacers range from metallic to extremely resistive and for all these spacers intensive antiferromagnetic coupling is already observed. In order to elucidate the mechanism of the interlayer coupling, we measured the temperature dependence of the magnetic and electric properties of $[\mathrm{Fe}(30\,\text{Å})/\mathrm{Fe}_{1-x}\mathrm{Si}_x(t_s\,\text{Å})]_{22}$ superlattices ($x=0.63$, 0.73, 1.00). For all these spacer compositions, no dramatic temperature dependence was found in the remanence ratio M_r/M_s of ferromagnetically coupled and noncoupled superlattices. In contrast, both M_r/M_s and H_s sensitively depend on the temperature and the spacer composition for AF coupled samples, as shown in Fig. 5. For $x=0.63$, M_r/M_s is independent of temperature and nearly equal to zero. For $x>0.63$, both M_r/M_s and H_s increases rapidly with decreasing temperature. den Broader and Kohlhepp found similar behaviors in Fe/Si superlattices.[19] They speculate that the increase of M_r/M_s with decreasing temperature is due to pinholes or (super)paramagnetic→magnetic transition of bridging regions. However, this effect seems to be not so serious for our samples, because we observed well-defined layered structures in our $\mathrm{Fe}/\mathrm{Fe}_{1-x}\mathrm{Si}_x$ superlattices, as shown in Fig. 6. If there is invisible direct connections between neighboring Fe layers, the temperature dependence of CPP resistivity should

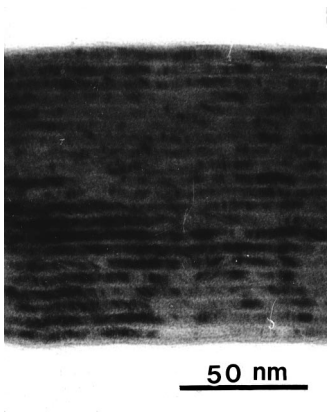

FIG. 6. Cross-sectional TEM micrograph of a $[\mathrm{Fe}(30\,\text{Å})/\mathrm{Fe}_{0.27}\mathrm{Si}_{0.73}(25\,\text{Å})]_{22}$ superlattice.

be metallic; namely, the resistivity should increase with increasing the temperature. But this is not the case for our samples, as will be described later. Recently, Kohlhepp *et al.*[20] reported that the high M_r/M_s due to an imperfect layered structure at the initial growth stage imitated an apparent strong biquadratic coupling. If their speculation is correct, M_r/M_s should decrease monotonically with increasing stacking number N. This is not the case for our present work, because our numerous experiments show that M_r/M_s remains constant at least for $N\geqslant 20$, as observed by Chaiken, Michel, and Wall.[7] Therefore, we believe that the somewhat large remanence of the $\mathrm{Fe}/\mathrm{Fe}_{1-x}\mathrm{Si}_x$ superlattices is not due to structural imperfection at the initial growth stage but due to the intrinsic biquadratic coupling nature of Fe/Si. Following this idea, Fullerton and Bader determined bilinear and biquadratic constants J_1, J_2 to fit observed magnetization curves.[8] We adopt the same approach to determine the coupling constants by using the following energy expression for a trilayer coupling system in Fig. 7:

$$E=-2M_s t_{\mathrm{Fe}}H\cos\theta-J_1\cos 2\theta-J_2\cos^2 2\theta, \qquad (1)$$

where θ denotes the angle between the external field and the magnetization, J_1 and J_2 are the bilinear and biquadratic coupling constants, respectively. The two coupling constants were determined by a precise fitting to all the magnetization curves measured at various temperatures. Figures 8(a)–8(c) show the temperature dependence of $J_1(T)$ and $J_2(T)$ for three kinds of $[\mathrm{Fe}(30\,\text{Å})/\mathrm{Fe}_{1-x}\mathrm{Si}_x(t_{\mathrm{AF}}\,\text{Å})]_{22}$ superlattices ($x=0.63$, 0.73, 1.00). For $x=0.63$, which was later found to be metallic from the measurement of the temperature depen-

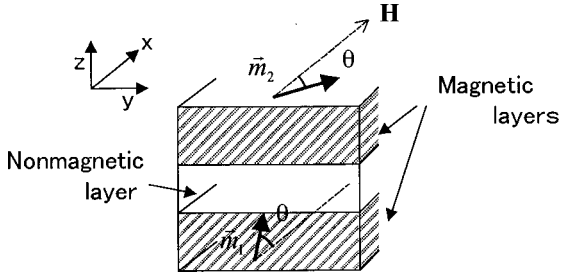

FIG. 7. A trilayer coupling model for the calculation of coupling constants J_1 and J_2.

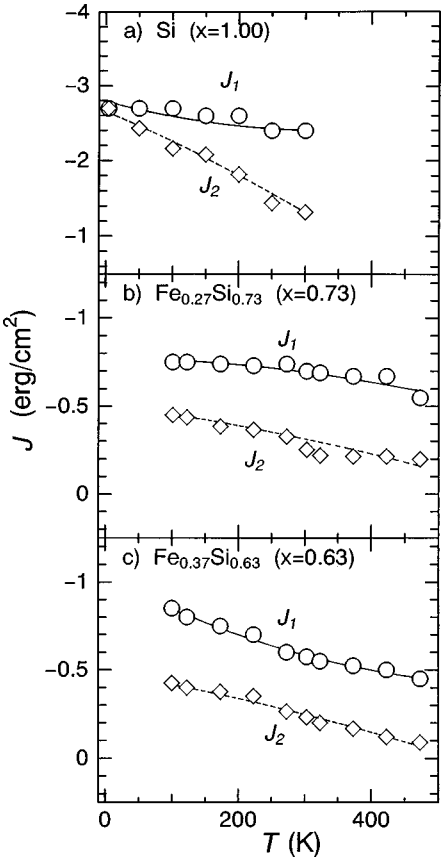

FIG. 8. Temperature dependence of the interlayer coupling constants J_1, J_2 of $[\mathrm{Fe}(30\,\text{Å})/\mathrm{Fe}_{1-x}\mathrm{Si}_x(t_{\mathrm{AF}}\,\text{Å})]_{22}$ ($x=0.63$, 0.73, 1.00) superlattices. The solid and dotted lines are guides to the eye.

dence of electric resistivity, both $|J_1|$ and $|J_2|$ decrease markedly with increasing the temperature [Fig. 8(c)]. In contrast, they become insensitive to temperature for $x \geqslant 0.73$. Thus, the magnitude and temperature dependence of interlayer coupling is very sensitive to the spacer composition. In order to investigate the electric properties of Fe/$Fe_{1-x}Si_x$ superlattices, we performed CIP and CPP resistivity measurements as a function of temperature. CIP resistivity for all spacer compositions showed monotonous increase with increasing the temperature in the range of 77–300 K, indicating that current mainly flows through metal Fe layers due to very high resistivity of $Fe_{1-x}Si_x$ spacers. In contrast with CIP resistivity, the temperature dependence of CPP resistivity greatly depends on the spacer composition, as shown in Fig. 9. For $x \leqslant 0.8$, the resistivity increases monotonically with the temperature, indicating that the spacer is metallic. In contrast for $x \geqslant 0.8$, the resistivity decreases slightly with increasing the temperature. This critical composition $x \sim 0.8$ for metal-to-insulator transition almost coincides with the value determined by the photoelectron spectroscopic methods.[21] Moreover, the formation of insulating layer in Fe/Si was recently reported by Kläsges *et al.* by means of spin- and angle-resolved photoemission spectroscopy.[22] They found that nonmagnetic and nonstoichiometric interdiffused layer which has zero density of states at the Fermi level is formed at the Fe/Si interface. Following the formation of such an insulating intermixed layer with thickness of about 4 ML (~6 Å), magnetic silicide (probably Fe_3Si) with a thickness of 6 ML and then α-Fe are successively formed.

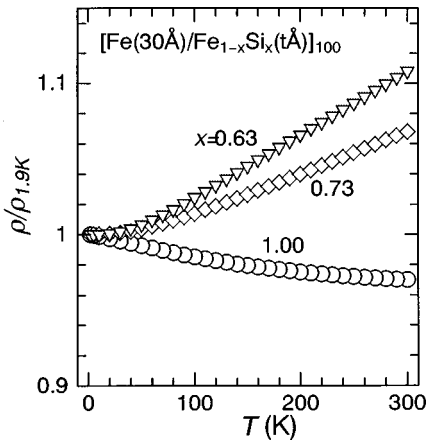

FIG. 9. Temperature dependence of electric resistivity for $[\mathrm{Fe}(30\,\text{Å})/\mathrm{Fe}_{1-x}\mathrm{Si}_x(t_{\mathrm{AF}}\,\text{Å})]_{100}$ ($x=0.63$, 0.73, 1.00) superlattices. $\rho_{1.9\,\mathrm{K}}$ is the resistivity at 1.9 K.

For Si on Fe, a metallic diffused layer with a thickness of 4 ML, an insulating diffused layer with 4 ML, and amorphous Si are successively grown on Fe. According to their precise surface analyses, it is highly probable that there exist insulating diffused layers in Fe/$Fe_{1-x}Si_x$ ($x \geqslant 0.8$). Moreover, Chubunova *et al.* found that no detectable intermixing occurred for Si on top of Fe.[23] All these precise surface analyses strongly suggest that a Fe/$Fe_{1-x}Si_x$ ($x \geqslant 0.8$) superlattice contains insulating spacer regions in it.

As mentioned above, the magnitude and temperature dependence of interlayer coupling is very sensitive to the spacer composition. We attempt to explain these temperature-dependent behaviors on the basis of a few theoretical models. Slonczewski proposed two coupling models. One is the ''thickness-fluctuation'' model,[24] in which a biquadratic coupling is assumed to be caused by spatial fluctuations of bilinear coupling due to thickness fluctuation of the spacer. The other is the ''*loose*'' spin model,[25] in which loose spins within each spacer or adjacent to ferromagnetic/nonmagnetic interfaces are assumed to mediate interlayer coupling. Since the latter is based on the RKKY (Rudermann-Kittel-Kasuya-Yoshida) theory, it is applicable only to a metallic spacer. It is found that the above two

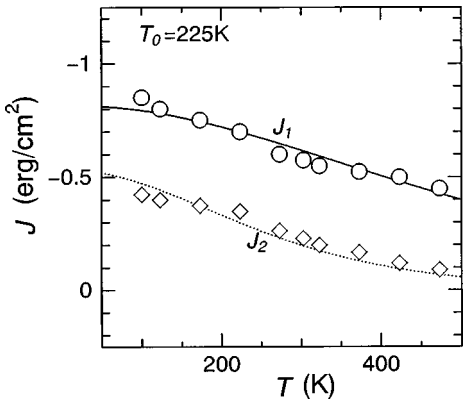

FIG. 10. Temperature dependence of the interlayer coupling constants J_1, J_2 for $[\mathrm{Fe}(30\,\text{Å})/\mathrm{Fe}_{1-x}\mathrm{Si}_x(t_{\mathrm{AF}}\,\text{Å})]_{22}$ ($x=0.63$) superlattices. Solid and dotted lines indicate the theoretically calculated J_1 and J_2 by quantum interference model. In the calculation, T_0 was set to 225 K as explained in the text.

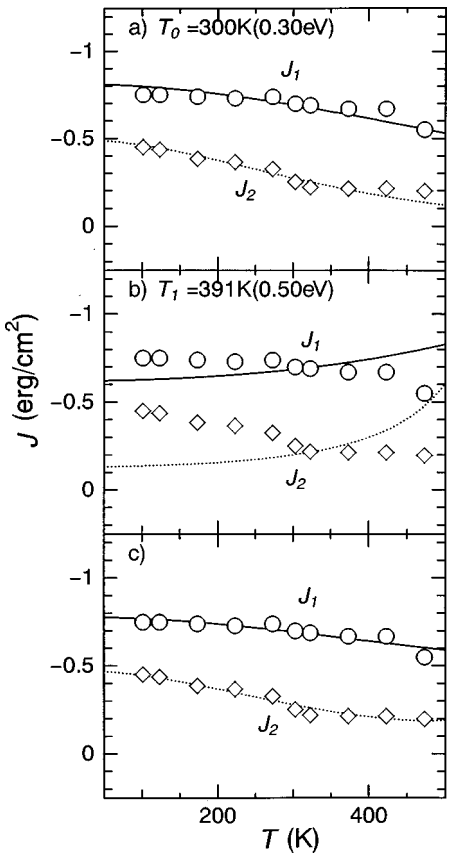

FIG. 11. Interlayer coupling constants J_1 and J_2 of a $[\mathrm{Fe}(30\,\text{Å})/\mathrm{Fe}_{1-x}\mathrm{Si}_x(t_{\mathrm{AF}}\,\text{Å})]_{22}$ ($x=0.73$) superlattice as functions of temperature. The solid and dotted lines, respectively, show the theoretically calculated coupling constants J_1 and J_2 by the interference model. A purely metallic spacer with $T_0=300$ K and a purely insulating spacer with $T_1=391$ K were assumed for (a) and (b), respectively. In (c), a mixture of the metallic and insulating regions were assumed. See the text for details.

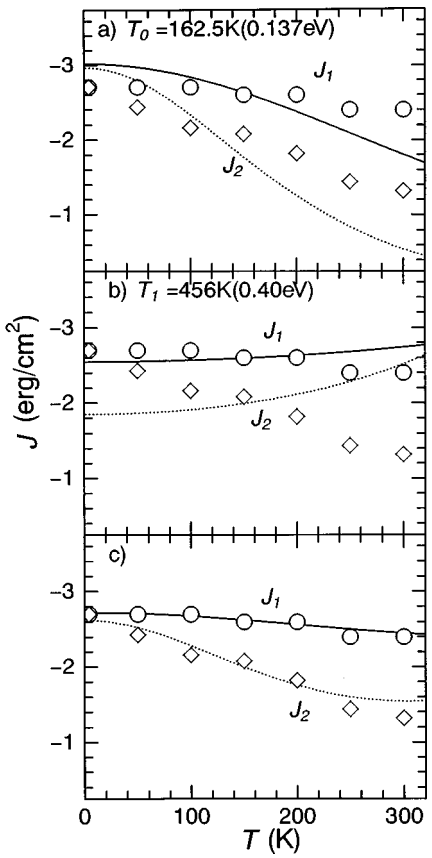

FIG. 12. Interlayer coupling constants J_1 and J_2 of a $[\mathrm{Fe}(30\,\text{Å})/\mathrm{Fe}_{1-x}\mathrm{Si}_x(t_{\mathrm{AF}}\,\text{Å})]_{22}$ ($x=1.00$) superlattice as functions of temperature. The solid and dotted lines, respectively, show the theoretically calculated coupling constants J_1 and J_2 by the interference model. A purely metallic spacer with $T_0=162.5$ K and a purely insulating spacer with $T_1=456$ K were assumed for (a) and (b), respectively. In (c), mixture of the metallic and insulating regions were assumed. See the text for details.

models gave no satisfactory explanations for the temperature dependences of $\mathrm{Fe}/\mathrm{Fe}_{1-x}\mathrm{Si}_x$ superlattices.[26] On the other hand, Bruno formalized interlayer exchange coupling based on the quantum interference model.[27] Depending on the position of the Fermi level (ε_F) against the potential of the spacer (U), the bilinear and biquadratic coupling J_1 and J_2 can be approximately given by

$$J_1'=J_{10}'\frac{(T/T_0)}{\sinh(T/T_0)},\quad J_2'=J_{20}'\frac{(2T/T_0)}{\sinh(2T/T_0)} \tag{2}$$

for a metallic spacer ($\varepsilon_F>U$), and

$$J_1''=J_{10}''\frac{(T/T_1)}{\sin(T/T_1)},\quad J_2''=J_{20}''\frac{(2T/T_1)}{\sin(2T/T_1)} \tag{3}$$

for an insulating spacer ($\varepsilon_F<U$). Here, J_{10}', J_{10}'', J_{20}', and J_{20}'' denote the coupling constants at $T=0$, and T_0 and T_1 are, respectively, given by

$$T_0=\frac{\hbar^2\sqrt{2m(\varepsilon_F-U)/\hbar^2}}{2\pi k_B m t_s},\quad T_1=\frac{\hbar^2\sqrt{2m(U-\varepsilon_F)/\hbar^2}}{2\pi k_B m t_s}, \tag{4}$$

where m is the effective electron mass. If a spacer is spatially inhomogeneous due to either compositional fluctuations or imperfect layered structures,[10] the spacer properties will vary with position. This can be theoretically treated by assuming that the spacer is a mixture of a metallic and an insulating compound. Thus the general expression for the bilinear coupling would be given by the superposition of Eqs. (2) and (3) as

$$\begin{aligned}J_1&=\lambda J_1'+(1-\lambda)J_1''\\&=\lambda J_{10}'\frac{(T/T_0)}{\sinh(T/T_0)}+(1-\lambda)J_{10}''\frac{(T/T_1)}{\sin(T/T_1)},\end{aligned} \tag{5}$$

where λ denotes the ratio of the metallic volume fraction to the total spacer volume. Similarly, the biquadratic coupling can be derived as

$$J_2=\lambda J_{20}'\frac{(2T/T_0)}{\sinh(2T/T_0)}+(1-\lambda)J_{20}''\frac{(2T/T_1)}{\sin(2T/T_1)}. \tag{6}$$

At first, we explain the temperature dependence of interlayer coupling of $\mathrm{Fe}/\mathrm{Fe}_{1-x}\mathrm{Si}_x$ ($x=0.54$, 0.63) superlattices. Since the $\mathrm{Fe}_{1-x}\mathrm{Si}_x$ spacer is purely metallic for these samples, Eq. (2) is applicable. By choosing the appropriate fitting param-

TABLE II. List of the fitting parameters by the quantum interference model.

	Metallic			Insulating		
Spacer	T_0	$\lambda J_{10}'$	$\lambda J_{20}'$	T_1	$(1-\lambda)J_{10}''$	$(1-\lambda)J_{20}''$
Si	162.5	−1.135	−1.861	456	−1.594	−0.777
$Fe_{0.27}Si_{0.73}$	300	−0.666	−0.459	391	−0.119	−0.018
$Fe_{0.37}Si_{0.63}$	225	−0.82	−0.53			

eter T_0, we can perfectly reproduce the experimental results, as shown in Fig. 10. Best fitting results were obtained at $T_0 \sim 100$ K for $x=0.54$ and 225 K for $x=0.63$. These values correspond with the energy difference $(\varepsilon_F - U)$ of 0.055 eV for $x=0.54$ and 0.219 eV for $x=0.63$ assuming that m is the free-electron mass. For $x=0.73$ which seems to be on the border of a metal-insulator transition, the coupling behaviors can be mostly described by Eq. (2), although there exists a slight deviation from the experiment [Fig. 11(a)]. This deviation indicates that Eq. (2) for a metallic spacer becomes gradually inadequate for larger x. For $x=1.0$ (pure Si), the deviation of Eq. (2) from the experiment becomes obvious, as shown in Fig. 12(a). It was also difficult to fit the experiment by using Eq. (3) which is the coupling expression for an insulating spacer [Fig. 12(b)]. However, the assumption of an inhomogeneous spacer structure [Eqs. (5) and (6)] can give a good fitting result as shown in Fig. 12(c). Here, we assumed that the energy gap of insulating region is nearly equal to that of amorphous Si ($E_g \sim 0.8$ eV); namely, $(U - \varepsilon_F) \sim 0.4$ eV which corresponds with $T_1 \sim 460$ K under the assumption of a free-electron mass. Since T_0 and T_1 determine the temperature-dependent behaviors, four unknown coefficients $\lambda J_{10}'$, $\lambda J_{20}'$, $(1-\lambda)J_{10}''$, and $(1-\lambda)J_{20}''$ were determined by the least-squares fitting at fixed T_0 and T_1. The fitting result is tabulated in Table II. Of course, there is some arbitrariness in the above fitting procedures, but the qualitative tendency of coupling behaviors in $Fe/Fe_{1-x}Si_x$ superlattices can be explained by the quantum interference model.

As mentioned above, the conductivity of the nonmagnetic $Fe_{1-x}Si_x$ ($x \geq 0.5$) layers ranges from metallic to insulating with increasing the Si content. All these spacer layers mediate interlayer coupling in $Fe/Fe_{1-x}Si_x$ superlattices, and their temperature dependences can be explained qualitatively by the quantum interference model formalized by Bruno.[27] The most striking feature of the $Fe/Fe_{1-x}Si_x$ superlattice is a dramatic enhancement of the interlayer coupling with increase of Si content. Figure 13 shows the coupling constants J_1 and J_2 of $[Fe(30\,\text{Å})/Fe_{1-x}Si_x(t_{AF})]_{22}$ as a function of x, where t_{AF} is the optimal spacer thickness for AF coupling ($t_{AF} \sim 15$ Å). And the value of the bilinear coupling in the AF coupled Fe/Si superlattice is about four times as large as that in Fe/Cr superlattices.[28] More detailed investigation of this interesting feature is now in progress.

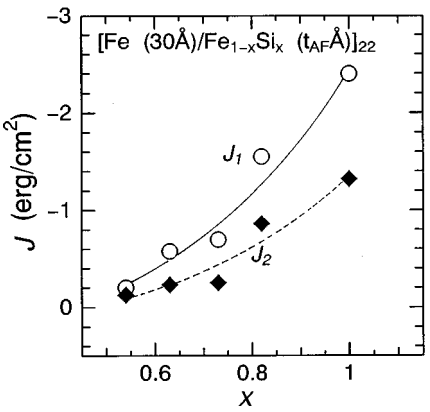

FIG. 13. Dependence of the interlayer coupling constants of $Fe/Fe_{1-x}Si_x$ superlattices on the composition (x) of the Fe-Si spacer. It is clearly noted that the increase in the Si content of the spacer greatly enhances the magnitude of the interlayer coupling. Empty circles (○) and solid diamonds (◆) indicate J_1 and J_2, respectively. The solid and dotted lines are guides to the eye.

IV. CONCLUSION

We have studied the exchange interlayer coupling of $Fe/Fe_{1-x}Si_x$ ($0.4 \leqslant x \leqslant 1.0$) superlattices. The $Fe_{1-x}Si_x$ spacer becomes nonmagnetic for $x \geqslant 0.5$ and changes from metallic to extremely resistive with increasing the Si content. For the whole spacer composition range above $x=0.5$, we have observed a strong interlayer coupling which changes from ferromagnetic to antiferromagnetic, and then noncoupling with an increase of the spacer layer thickness. Furthermore, these results indicate that both metallic and extremely resistive $Fe_{1-x}Si_x$ can mediate the interlayer coupling. The temperature dependence of the interlayer coupling behaves differently depending on the spacer composition; namely, the bilinear and biquadratic coupling constants, J_1 and J_2, decrease markedly with increasing temperature when the spacer is metallic, while the change becomes small when the spacer becomes almost insulating. The temperature dependence can be explained qualitatively by the quantum interference model proposed by Bruno. Furthermore, we found a dramatic enhancement of the interlayer coupling with the increase of Si content x, although the reason is yet to be clarified.

ACKNOWLEDGMENTS

Y.E. acknowledges financial support by the Storage Research Consortium in Japan. We are greatly indebted to M. Ichijo, H. Daimon, T. Maro, A. Yano, and K. Kawajiri for performing magnetic measurements, TEM, and electron diffraction. The low-angle XRD measurements were performed at the Laboratory for Developmental Research of Advanced Materials, the Institute for Material Research, Tohoku University. This work is supported by Research for the Future Program of Japan Society for the Promotion of Science under Grant No. 97R14701.

*Author to whom correspondence should be addressed. Electronic address: endo@rism.tohoku.ac.jp

[1] P. Grunberg, R. Schreiber, Y. Pang, U. Walz, M. B. Brodsky, and H. Sowers, J. Appl. Phys. **61**, 3750 (1987).

[2] S. S. P. Parkin, N. More, and K. P. Roche, Phys. Rev. Lett. **64**, 2304 (1990).

[3] S. Toscano, B. Briner, H. Hopster, and M. Landolt, J. Magn. Magn. Mater. **114**, L6 (1992).

[4] B. Briner and M. Landolt, Phys. Rev. Lett. **73**, 340 (1994).
[5] M. Xiao and Z. Li, Phys. Rev. B **54**, 3322 (1996).
[6] E. E. Fullerton, J. E. Mattson, S. R. Lee, C. H. Sowers, Y. Y. Huang, G. Felcher, S. D. Bader, and F. T. Parker, J. Magn. Magn. Mater. **117**, L301 (1992).
[7] A. Chaiken, R. P. Michel, and M. A. Wall, Phys. Rev. B **53**, 5518 (1996).
[8] E. E. Fullerton and S. D. Bader, Phys. Rev. B **53**, 5112 (1996).
[9] J. J. de Vries, J. Kohlhepp, F. J. A. den Broeder, R. Coehoorn, R. Jungblut, A. Reinders, and W. J. M. de Jonge, Phys. Rev. Lett. **78**, 3023 (1997).
[10] Y. Endo, O. Kitakami, and Y. Shimada, J. Magn. Soc. Jpn. **21**, 541 (1997).
[11] Y. Endo, O. Kitakami, and Y. Shimada, Appl. Phys. Lett. **72**, 495 (1998).
[12] K. Inomata, K. Yusu, and Y. Saito, Phys. Rev. Lett. **74**, 1863 (1995).
[13] Y. Fujii, *Metallic Superlattices*, edited by T. Shinjo and T. Takada (Elsevier, Amsterdam, 1987), p. 33.
[14] B. D. Cullity, *Elements of X-Ray Diffraction* (Addison-Wesley, Reading, MA 1956), p. 263.
[15] A. Barthelemy, A. Fert, M. N. Baibich, S. Hadjoudj, F. Petroff, P. Etienne, R. Cabanel, S. Lequien, F. Nguyen Van Dau, and G. Creuzet, J. Appl. Phys. **67**, 5908 (1990).
[16] B. Heinrich S. T. Purcell, J. R. Dutcher, K. B. Urquhart, J. F. Cochran, and A. S. Arrott, Phys. Rev. B **38**, 12 879 (1988).
[17] Y. Endo (unpublished).
[18] J. A. Carlisle, A. Chaiken, R. P. Michel, L. J. Terminello, J. J. Jia, T. A. Callcott, and D. L. Ederer, Phys. Rev. B **53**, R8824 (1996).
[19] F. J. A. de Broeder and J. Kohlhepp, Phys. Rev. Lett. **75**, 3026 (1995).
[20] J. Kohlhepp, M. Valkier, A. van der Graaf, and F. J. A. de Broeder, Phys. Rev. B **55**, R696 (1996).
[21] R. Kilper, St. Teichert, Th. Franke, P. Häussler, H.-G. Boyen, A. Cossy-Favre, and P. Oelhafen, Appl. Surf. Sci. **91**, 93 (1995).
[22] R. Kläsges, C. Carbone, W. Eberhardt, C. Pampuch, O. Rader, T. Kachel, and W. Gudat, Phys. Rev. B **56**, 10 801 (1997).
[23] E. V. Chubunova, I. D. Khabelashvili, Yu. Yu. Lebedinskii, V. N. Nevolin, and A. Zenkevich, Thin Solid Films **247**, 39 (1994).
[24] J. C. Slonczewski, Phys. Rev. Lett. **67**, 3172 (1991).
[25] J. C. Slonczewski, J. Appl. Phys. **73**, 5957 (1993).
[26] Y. Endo, O. Kitakami, and Y. Shimada, IEEE Trans. Magn. **34**, 906 (1998).
[27] P. Bruno, J. Appl. Phys. **76**, 6972 (1994).
[28] R. W. Wang, D. L. Mills, E. E. Fullerton, J. E. Mattson, and D. Bader, Phys. Rev. Lett. **72**, 920 (1994).